Does the coupling of the semiannual oscillation with the quasi-biennial oscillation provide predictability of Antarctic sudden stratospheric warmings?

Viktoria J. Nordström[1] and Annika Seppälä[1]

[1]Department of Physics, University of Otago, Dunedin, New Zealand

Correspondence: Annika Seppälä (annika.seppala@otago.ac.nz)

Abstract. During September 2019 a minor sudden stratospheric warming took place over the Southern Hemisphere (SH), bringing disruption to the usually stable winter vortex. The mesospheric winds reversed and temperatures in the stratosphere rose by over 50 K. Whilst SSW in the SH are rare, with the only major SSW having occurred in 2002, the Northern Hemisphere experiences about six per decade. Amplification of atmospheric waves during winter is thought to be one of the possible trigger SSWs, although other mechanisms are also possible. Our understanding, however, remains incomplete, especially with regards to SSW occurrence in the SH. Here, we investigate the effect of two equatorial atmospheric modes, the Quasi Biennial Oscillation (QBO) at 10 hPa and the Semiannual Oscillation (SAO) at 1 hPa during the SH winters of 2019 and 2002. Using MERRA-2 reanalysis data we find that the easterly wind patterns resembling the two modes merge at low latitudes in the early winter, forming a zero wind line that stretches from the lower stratosphere into the mesosphere. This influences the meridional wave guide, resulting in easterly momentum being deposited in the polar atmosphere throughout the polar winter, decelerating the westerly winds in the equatorward side of the polar vortex. As the winter progresses, the momentum deposition and wind anomalies descend further down into the stratosphere. We find similar behaviour in other years with early onset SH vortex weakening events. The magnitude of the SAO and the timing of the upper stratospheric (10 hPa) easterly QBO signal, was found to be unique in these years, when compared to the years with a similar QBO phase. We were able to identify the SSW/weak vortex years from the early winter location of the zero wind line at 1 hPa together with Eliassen-Palm flux divergence in the upper stratosphere at 40°S-50°S. We propose that this early winter behaviour resulting in deceleration of the polar winds may precondition the Southern atmosphere for a later enhanced wave forcing from the troposphere, resulting in a SSW/vortex weakening event. Thus the early winter equatorial upper stratosphere-mesosphere together with the polar upper atmosphere may provide early clues to an imminent SH SSW.

1 Introduction

During the austral winter of 2019, the Southern Hemisphere experienced a minor sudden stratospheric warming (SSW) (for a recent comprehensive review on SSWs see Baldwin et al., 2021, and references therein): Between September 5-11 temperatures in the Antarctic stratosphere at 10 hPa warmed by 50 K (Yamazaki et al., 2020). Furthermore, the polar zonal mean zonal winds

reversed, and the easterlies around 60°S at 10 hPa reached ∼60 ms^{-1} around September 16 (Rao et al., 2020c). The drivers of this minor SSW have been attributed to enhanced stationary planetary wave activity (Yamazaki et al., 2020).

The impacts of SSWs can influence the atmosphere from the polar region to mid-latitudes for months (see e.g. Baldwin and Dunkerton, 2001). For example, SSWs contribute to the size of the ozone hole via two different mechanisms. First, the warming of the stratosphere suppresses the formation of polar stratospheric clouds (Shen et al., 2020), which play a critical part in stratospheric ozone depletion (Solomon, 1999). Furthermore, the weakening of the vortex allows the mixing of ozone rich mid-latitude air into the pole. Both these effects in combination lead to a smaller ozone hole (Solomon et al., 1986). The anomalous winds from SSWs can also influence stratosphere-troposphere coupling, impacting the Southern and Northern Annular Modes (SAM and NAM) (Taguchi and Hartmann, 2005; Shen et al., 2020; Baldwin et al., 2021; Rao et al., 2020a).

In 2019, the SSW's influence cascaded down through the atmosphere for months following its occurrence. The minor SSW pushed the SAM into a negative phase (Rao et al., 2020c), signifying a shift of polar westerlies towards the equator (Doddridge and Marshall, 2017). This movement of strong westerly winds is believed to have impacted the Australian wildfires, which began in the following November (Lim et al., 2019). Furthermore, the changes in polar temperatures and winds shrunk the ozone hole to its smallest size ever observed (Eswaraiah et al., 2020a). Most of our understanding about SSWs comes from their occurrence over in the Northern Hemisphere (NH), where they take place almost every other year (Charlton and Polvani, 2007). Due to the rarity of SH SSW events (Rao et al., 2020c), the 2019 case provides a unique opportunity to investigate the atmospheric conditions leading up to SH SSWs.

SSWs in the Southern Hemisphere are infrequent. The most notable occurred in September 2002 (Allen et al., 2003), when the vortex shifted off the pole and eventually split into two. Later, one piece reformed into a weakened polar vortex (Ricaud et al., 2005). This impacted the ozone hole, which experienced 20% less ozone loss compared to previous years (Hoppel et al., 2003). An earlier SSW has been reported to have occurred in August-September 1988 (Schoeberl et al., 1989; Kanzawa and Kawaguchi, 1990). While it is unclear if this even filled the The World Meteorological Organization (WMO) criteria for major or minor (Charlton and Polvani, 2007) SSW, Thompson et al. (2005); Kwon et al. (2020) have found this event to be one of the larger, early polar vortex weakening events.

In September 2019 a SSW occurred again. Within days, temperatures in the stratosphere increased by 50 K (Yamazaki et al., 2020). Whilst the 2002 SSW was classified as major, according to the WMO definition, the 2019 event was minor (Yamazaki et al., 2020). Due to their rarity, the causes of a SSW in the SH are not well understood. Eswaraiah et al. (2016, 2020a, b) have further reported a minor SH warming in September 2010. Whilst the 2019 and 2010 are both deemed minor, their dynamics were very different. The 2010 event included a reversal of the temperature gradient poleward of 60°S from September 15, and the temperature increased by about 30 K at 80°S and 10 hPa (Eswaraiah et al., 2018). The zonal winds at 60°S at 10 hPa weakened by only 20-25 ms^{-1} (Eswaraiah et al., 2016). Hence, the dynamical situation in 2010 was unlike those in 2002 and 2019, because in the latter two years, rapid warmings and wind reversals occurred. Instead of the WMO criteria, for example Kwon et al. (2020) have identified southern stratospheric polar vortex weakening events, showing that these happen more frequently than SSW events and with an increasing occurrence frequency since the 2000s.

It is widely thought that SSWs are the product of an interaction between planetary waves and the atmospheric mean flow (Matsuno, 1971). NH has higher winter planetary wave activity and variability than the SH, thus leading to higher SSW occurrence in the NH. de la Cámara et al. (2019) have reported that about one third of sudden stratospheric deceleration events (events similar to SSWs) are preceded by anomalous wave activity from the troposphere. In two thirds of the events, the anomalous amplification of wave activity in the stratosphere that lead to the events, did not originate from the troposphere, but was likely linked to dynamics in the lower stratosphere and vortex geometry. As discussed by the recent comprehensive review of Baldwin et al. (2021, and references therein), the occurrence of SSW may be linked to various large scale oscillation modes in the atmosphere, including the Quasi-Biennial Oscillation (QBO, see e.g. Anstey and Shepherd (2014)), the Semiannual Oscillation (SAO), the El Ninõ-Southern Oscillation (ENSO, see e.g. Domeisen et al. (2019b)), the Madden Julian Oscillation (MJO, see e.g. Wheeler and Hendon (2004); Schwartz and Garfinkel (2017)), solar cycle, and extratropical blockings. Rao et al. (2019) also discuss these in detail, and provide an analysis of how each provided favourable conditions in the case of the NH 2019 SSW. Here, we will focus on the QBO and SAO in the SH context, and will not consider the others in detail.

The QBO is manifested in the reversal of zonal winds in the equatorial stratosphere. The eastward and westward winds alternate every 22-34 months, with an average period of 28 months (Baldwin et al., 2001). This oscillation dominates the variability of the equatorial stratosphere, however, its influence stretches to both poles (Baldwin et al., 2001). The phases of the QBO have been found to influence the polar vortex and occurrence of NH SSWs. Holton and Tan (1980) were the first to propose that the QBO at 40-50 hPa modulates the subtropical zero wind line, which influences the propagation on waves in the stratosphere – a phenomenon known as the Holton-Tan effect (see Watson and Gray, 2014, and references therein). It was later discovered (concerning the NH) that the easterly QBO phase coincides with more SSWs (Richter et al., 2011). Other known nonlinear interactions with the QBO and SSW occurrence in the NH include those with the solar cycle (Labitzke, 2005) (for QBO at 45 hPa). Due to the scarcity of SH SSW events, similar relationships connecting the solar cycle, QBO and SSW occurrence have not been identified.

The Semiannual Oscillation is an alternation of zonal winds in the equatorial mesosphere. These winds swap between westerly and easterly, with a complete cycle taking six months. These wind shears descend down from above the mesopause into the upper stratosphere (Kawatani et al., 2020). The SAO amplitude has two peaks: one near the stratopause (1 hPa) and another close to the mesopause (0.01 hPa) (Kawatani et al., 2020). Westerlies near the stratopause maximise close to the equinoxes, whilst the easterlies maximise near the solstices. The SAO maxima at 1 hPa exhibit a seasonal asymmetry, where the 'first cycle', which begins in December with the NH easterly phase, is stronger than the 'second cycle', which starts with the SH easterly, roughly in June (Garcia et al., 1997; Peña-Ortiz et al., 2010). This behaviour arises from differences in extra tropical wave forcing, which is generally understood to be stronger in the NH winter (Garcia et al., 1997). The drivers of the SAO are not well understood. The prevailing theories suggest that the westerly accelerations, in March and September, are caused by Kelvin and high frequency gravity waves, whilst the easterlies maximise, during December and June, from advection of easterly momentum across the Equator, by the upper branch of the Brewer-Dobson circulation (Smith et al., 2020).

Recent work by Gray et al. (2020) noted the importance of the equatorial mesosphere and upper stratosphere on forecasting Northern Hemisphere SSWs. Their modelling study showed that SSWs were only reproduced realistically when the flow in the

equatorial upper stratosphere was constrained, simulating the two atmospheric modes in this region, the SAO and the QBO. Similar results were previously presented by Pascoe et al. (2006): In a troposphere-stratosphere-mesosphere global circulation model with forced QBO and SAO like variability, the timing of the NH mid winter warming advanced by about one month.

Whilst many studies have investigated the troposphere for answers to the questions raised by SSWs, we are here following suggestions that the upper atmosphere may be key to understand the drivers of SSWs. The works of Pascoe et al. (2006) and Gray et al. (2020) discussed above, draw attention to the upper atmosphere in the formation of a SSW, with a focus on the NH. In the present study, we analyze the behaviour of the QBO and SAO in the Southern Hemisphere during the winters of 2002 and 2019 and two additional weak vortex event years, based on reanalysis data.

2 Data and Methods

2.1 MERRA-2

The second Modern-Era Retrospective analysis for Research and Applications (MERRA Version 2, MERRA-2) is a National Aeronautics and Space Administration (NASA) atmospheric reanalysis product that begins in 1980 (Bosilovich et al., 2016). MERRA-2 has a horizontal resolution of $0.5^\circ \times 0.625^\circ$ with 42 levels in the vertical from the surface to 0.01 hPa (Gelaro et al., 2017).

To investigate the connections between the SAO, QBO and SSW we used the four-times-daily zonal wind, geopotential height and temperature information of MERRA-2, averaged into daily means. We focus on the vertical pressure range of 550 to 0.1 hPa and the austral winter (June-September). Our analysis focuses mainly on the years 2019 and 2002, when SSW events took place in the Southern Hemisphere.

2.2 Semiannual Oscillation

Here, we focus our investigation on the easterly SAO maxima that occurs in the upper stratosphere, close to 1 hPa. The SAO is locked into the seasonal cycle (Kawatani et al., 2020), and is known to have a period of six months, but it has appreciable inter-annual variability (Smith et al., 2020). Smith et al. (2017) report from multiyear satellite observations that the first easterly maxima, which occurs during the Northern Hemisphere winter has climatological equatorial zonal mean zonal winds between 20-30 m/s at 1 hPa, while the second maxima, occurring during the Southern Hemisphere winter, these peak between 0-20 m/s.

At 1 hPa MERRA-2 has been found to represent the easterly SAO in qualitative agreement with satellite derived winds (Kawatani et al., 2020). However, MERRA-2 has westerly bias compared to other reanalysis data and observations above 20 hPa. For the months considered here (June-September), Kawatani et al. (2020) show that the interannual variability in MERRA-2 SAO is comparable to other reanalysis data sets, suggesting that for our analysis, changes from year to year should be captured at a reasonable level.

For our analysis, will calculate the SAO equatorial wind amplitude at 1 hPa level by averaging over the equatorial latitudes 5°S–5°N from June to September. We will further estimate how far into the Southern Hemisphere the easterly wind pattern extends by finding the latitudinal location where the easterly winds turn westerly.

2.3 Quasi-biennial Oscillation

Here, we focus on years with easterly QBO (eQBO) phase in the equatorial upper stratosphere zonal mean zonal wind during June-July. Analogously to Rao et al. (2020c), we take the QBO phase at the 10 hPa pressure level, which Rao et al. (2020c) have shown to provide favourable conditions for SSW occurrence the SH. QBO structure and dynamics in MERRA-2 reanalysis are discussed in detail by Coy et al. (2016), who conclude that MERRA-2 displays a realistic QBO behaviour. We verified this by contrasting the zonal winds to radiosonde measurements from Singapore and found the two to be consistent, as expected (Coy et al., 2016).

For this study, eQBO is taken to be present if the mean June–July 10 hPa equatorial (5°S–5°N) zonal mean flow is easterly. The years fulfilling these conditions are 1980, 1983, 1985, 1988, 1990, 1993, 1995, 1997, 1999, 2002, 2004, 2006, 2008, 2011, 2014, 2017, and 2019. We will discuss magnitudes of the eQBO winds during the eQBO years in the following sections.

To contrast the SSW years of 2019 and 2002 to others with similar large scale equatorial flow conditions, other years with equivalent, i.e. eQBO phase, conditions during the austral winter months were analysed as a reference. Additionally, for the reference dataset, we leave out the early onset date (August onset) weak vortex years of 1988 and 2017 (Kwon et al., 2020). Thus, the 13 reference eQBO years in the MERRA-2 period are 1980, 1983, 1985, 1990, 1993, 1995, 1997, 1999, 2004, 2006, 2008, 2011, and 2014.

All years were initially analysed separately to check for conditions similar to year 2002 and 2019. As noted above, the years 1988 and 2017 were considered separately from the reference data set, due to the early vortex weakening events. In 2017 the polar vortex has been reported to have experienced a disruption due to enhanced planetary wave activity throughout winter (Klekociuk et al., 2020). This lead to a smaller than average spring ozone hole (Klekociuk et al., 2020). There have also been reports of a SSW occurrence in 1988 (Schoeberl et al., 1989; Kanzawa and Kawaguchi, 1990), however, Thompson et al. (2005); Kwon et al. (2020) find this year to rather correspond to a weak vortex, wather than fulfilling SSW criteria.

2.4 Wave propagation

We use the quasi-geostrophic Eliassen-Palm flux (EP flux) to visualise wave propagation and momentum deposition (as indicated by the divergence of the EP flux). Stationary and transient wave components are not separated, rather we analyse the total contribution from both. The convergence (negative values) and divergence (positive values) of the EP flux correspond to deceleration and acceleration of zonal westerly winds respectively. The EP flux results shown here were calculated from the MERRA-2 data according to Edmon et al. (1980), with additional scaling for display purposes as described by Bracegirdle (2011).

Figure 1 presents the 7-day averages of zonal mean zonal wind (ms^{-1}), EP flux (arrows, m^2s^{-2}, reference arrow shown in the first panel) and EP flux divergence (grey contours, ± 2 $ms^{-1}day^{-1}$ contours levels included) averaged for the reference

years 1980, 1983, 1985, 1990, 1993, 1995, 1997, 1999, 2004, 2006, 2008, 2011, and 2014. The MERRA-2 zonal mean zonal wind reaches westerly velocities of over 100 ms^{-1} in the polar vortex in the upper stratosphere around 1 hPa in June-July, after which the wind maximum descents down towards 10 hPa, with peak velocities of 70 ms^{-1} by mid-September. Consistent with the selection of eQBO years, we can see the easterly wind signature at 10 hPa at the equator, persisting throughout the time period and remaining well below the 1 hPa level. The easterly SAO wind pattern presents at around 1 hPa from June to early July, after which it subsides as the SAO annual cycle shifts to westerlies (Kawatani et al., 2020). There is no clear merging of the eQBO and SAO wind structures. The figures also indicate the location where the zonal winds changes from easterly to westerly with a black solid contour (0 ms^{-1}, zero wind line). Propagation of stationary waves requires westerly flow, thus the zero wind line forms a barrier for stationary wave propagation.

The EP flux and its divergence indicate that from June to early-July the waves are generally acting to accelerate the zonal flow in the poleward side of the polar vortex and decelerating it on the equatorward side. This deceleration happens more consistently from mid-July onwards, at the same time as wave propagation upwards and equatorwards is enhanced above 100 hPa. The zero wind line at 10 hPa is initially located between 10°S-20°S, extending to 30°S from mid-August.

3 Results

3.1 SH polar winter 2019

Figure 2 shows how the 7 day averaged zonal mean zonal wind evolves with time, along with the propagation of planetary scale waves during the austral winter of 2019, with the EP flux arrows illustrating the direction of wave movement. Presentation and timing is analogous to Figure 1. As before, the location of the zero wind line (contour of 0 ms^{-1} zonal mean zonal wind) is indicated as a thick black line. The EP flux divergence is shown with the grey dashed line indicating where the waves dissipate and deposit easterly momentum to atmospheric flow, acting to decelerate it at a rate of 2 $ms^{-1}day^{-1}$, and the grey solid line indicating where acceleration is taking place at a rate of 2 $ms^{-1}day^{-1}$.

Throughout the winter, the equatorial atmosphere around 10 hPa shows a easterly zonal mean zonal wind structure, with peak velocities of 30-40 ms^{-1}, indicating the presence of QBO in the easterly phase. This eQBO wind signal is present around 10 hPa from early June, and is not initiated by the descending easterly SAO (seen here above 1 hPa), as may happen with wQBO (Kuai et al., 2009). Contrasting to the reference (Figure 1), the equatorial SAO around 1 hPa is evident from mid-June, with zonal mean zonal winds of up to -20-30 ms^{-1}. The easterly wind structure extends further into the Southern Hemisphere (20°S by late June) than in the reference, and persists into mid-July, when it merges with the easterly wind structure that originates from the 10 hPa eQBO easterly wind structure.

From mid-June onwards, enhanced upwards wave propagation is taking place above 10 hPa and the wave convergence is driving enhanced deceleration on the equatorward side of the polar vortex. This can be seen clearly in Figure 3, which presents the 2019 anomaly relative to the reference mean ("Figure 2" - "Figure 1"). Unlike in late-August, when enhanced upwards wave flux originating from the troposphere (Eswaraiah et al., 2020a; Shen et al., 2020; Yamazaki et al., 2020) is taking place across the stratosphere, the earlier enhanced upwards flux is limited to 10 hPa and above.

Initially in early June, enhanced easterly momentum deposition is taking place between 40°S-60°S, decelerating the flow above 1 hPa. This extends downwards and equatorwards, resulting in consistent deceleration of the upper stratospheric flow between 20°S-50°S from mid-June throughout July. At the same time the zonal wind is accelerated by 10-20 ms^{-1} around 60°S. This leads to a more vertically aligned structure of the polar vortex zonal mean zonal wind, rather than the typical structure, which we can see in Figure 1, tilted towards equator in the upper stratosphere. This appears to correspond a vortex shape Albers and Birner (2014) found typical for NH split type SSW events.

From late-June the direction of wave propagation in the upper stratosphere is guided by the easterly wind structure near 1 hPa. By early-July the convergence of the EP flux contributes to deceleration of the stratospheric flow above 10 hPa around 20°S, leading to a structure that resembles merging of the previously separate easterly wind structures of the SAO and eQBO. The formed zero wind line guides more wave upwards. Through out July and into August the zonal mean zonal wind is consistently weaker by 10-20 ms^{-1} across the stratosphere between latitudes of 60°S and 40°S. By late-August, when we observe enhanced upwards wave propagation from the troposphere, the zonal flow is further rapidly decelerated above 10 hPa, leading to the SSW conditions in September.

3.2 SH polar winter 2002

Figures 4 and 5 are analogous to Figures 2 and 3 but now for the austral winter of 2002. Again we observed the eQBO wind structure at 10 hPa from early June, similar to 2019. From June 8 onwards, the easterly oscillation of the SAO is present around 1 hPa and upwards wave propagation is enhanced throughout the stratosphere above 100 hPa. Between about 40°S and 60°S enhanced easterly momentum deposition throughout the atmosphere above 10 hPa, lead to deceleration of the zonal winds in this region throughout the time period. As in the case of the winter of 2019, we see a merging of the previously separate easterly wind structures of the SAO and eQBO. This now takes place mid-June, approximately four weeks earlier than in 2019. The zero wind line of the zonal mean zonal wind, formed as a result, extends to 30°S, cutting across $\sim$0.4–30 hPa.

This vertical extend is not maintained for extended periods of time. However, as in 2019, the latitudinal location of the zero wind line between 1–50 hPa is shifted about 10 degrees polewards from its typical location (Figure 1) throughout July, to about 30°S.

In both cases, the merging of the two initially separate easterly wind patterns, the resulting shift in the zero wind line across the month of July, well before the SSW onsets took place in September, and the enhanced zonal flow deceleration above 10 hPa appear notable.

Overall, the atmospheric response above 10 hPa is remarkably similar to 2019: Both years show sustained wave driven deceleration of zonal mean wind between 40°S-60°S from June, throughout July, and simultaneous acceleration between about 60°S-70°S. By early to mid-August the zonal winds have decelerated across the polar region above 1 hPa.

Identical analysis for the previously identified early weak vortex event years of 1988 and 2017 show that a similar equatorial easterly wind pattern mergers took place during both winters (figures included as supplement). In 2017 this happened in late June, accompanied by enhanced upwards EP flux, and followed by a poleward shift in the zero wind line latitudinal location.

In 1988 this happened much later, from 20 July onwards. In 1988, however, there is no indication of enhanced upwards wave propagation in June, as was the case for 2002, 2017, and 2019.

3.3 Weak vortex events in context of other eQBO years

When analysing all the eQBO years individually the type of equatorial wind pattern merger reported above either did not take place, or took place much later, and, like in 1988 was not accompanied by enhanced upwards wave flux.

Based on these results it appears that for the SSW cases and the weak vortex cases, there is an interplay of early winter wave forcing and the wave guide formed by the zonal mean zonal wind structures to do with the equatorial easterly winds related to the SAO around 1 hPa and the equatorial easterly winds related to the QBO around 10 hPa. We will now proceed to investigate if these factors together provide predictability for the weak vortex events.

The top left panel in Figure 6 presents the temporal evolution of the 7-day mean magnitude of the equatorial zonal mean zonal wind averaged over 5°S-5°N for the 1 hPa level, representing the upper stratospheric SAO. The years 1988, 2002, 2017, and 2019 have been labeled separately, while all other eQBO years are shown as grey lines. Years 2002, 2017, and 2019 have some of the highest easterly wind velocities reaching 10 ms^{-1} and higher in June. In this context we should note again that the results of Kawatani et al. (2020) suggest that interannual variability in MERRA-2 is consistent with other reanalysis datasets, but that MERRA-2 has a westerly bias above 20 hPa. The year when the June velocities reach -30 ms^{-1} corresponds to the first MERRA-2 year, 1980.

The bottom left panel presents a similar zonal wind temporal evolution (averaged over 5°S-5°N), but now for the QBO level of 10 hPa. Again, the years 2002, 2017, and 2019 show some of the largest easterly velocities, between -20– -40 ms^{-1} in June-July. While the SAO is known to occur regularly, but with appreciable inter-annual variability (Smith et al., 2020), as we seen in Figure 6, the QBO on the other hand has an average period of 28 months. We can see this in the temporal evolution of the equatorial 10 hPa winds: in some cases the winds remain westerly for much of June before shift to the easterly phase, while in 1988, the phase changes from easterly to westerly in July.

The panels on the right hand side of Figure 6 show the mean and median latitudinal locations of the zero wind line (zero U) at 1 hPa (top) and 10 hPa (bottom). The grey error bars indicate one standard deviation ($1 \times \sigma$) around the mean latitudinal location. As before the years 1988, 2002, 2017, and 2019 have been labeled separately.

At 1 hPa, the years 2002, 2017, and 2019 all show significant (beyond $2 \times \sigma$) southward shift of the location where winds turn from westerly to easterly in the meridional direction. While the mean location remains close to the equator, for 2002, 2017, and 2019 we see a shifts to locations between 15°S and about 27°S. This takes place in June, while for 1988, the shift is seen later at a time when there is in general more variability as shown by the large $1 \times \sigma$ bar.

At 10 hPa there is not as clear of a shift as we see at 1 hPa. However, in all cases the latitudinal location where the 10 hPa winds change direction is preferably in the SH poleward range, between 18°S and 30°S in June-July. This could suggest that the SSW events in the SH are sensitive to the timing of the eQBO phase during the polar winter.

Considering the shift in the location of the zero wind line at 1 hPa, we now examine if this could be used with a measure of the wave forcing to identify SH SSW/weak vortex events. Figure 7a) shows the upper stratospheric EP flux divergence

on the equator side of the polar vortex edge (see Figure 1), averaged between 1-10 hPa and between latitudes 50°S-40°S (in units of $\mathrm{ms}^{-1}\mathrm{day}^{-1}$) versus the average latitude of the zero wind line at 1 hPa. Both variables are averaged from mid-June to mid-July, identified as a potential key timing from Figure 6. In Figure 7b) the averaging period is shifted by 14 days to 29 June–26 July. For each of the following panels the zero wind line averaging time periods remain the same in the respective columns, while the averaging period of the EP flux divergence changes, as given in the panel title. Panels c) to f) correspond to the lower stratospheric EP flux divergence, again on the equator side of the polar vortex edge, now averaged for 50-70 hPa and 60°S-40°S.

In mid-June to mid-July in the upper stratosphere (Figure 7a) in mid-June to mid-July the zero wind line is located north of the equator, but has moved clearly southward in 2002 and 2019, with EP flux divergence between -3 to -2.5 $\mathrm{ms}^{-1}\mathrm{day}^{-1}$. We also see a large southward shift of over 10° in 1980, 1990, and 2017, but these years no not exhibit similar zonal flow deceleration from wave forcing. As discussed earlier, the year 1980 had the largest amplitude of the SAO zonal wind (Figure 6), and upon further investigation, the year 1990 is also amongst the large June amplitude SAO wind years, with peak wind easterly velocities of 10-15 ms^{-1}. Both however, have a changing 10 hPa QBO phase in June, unlike 2002, 2017 and 2019 which show eQBO from start of June. This suggest that the SAO amplitude alone is not sufficient to understand later vortex weakening events, but should be viewed in context of the QBO phase in early winter.

Shifting the time period later (Figure 7b), now shows a similar response for the year 2017, with an average zonal flow deceleration of over 4 $\mathrm{ms}^{-1}\mathrm{day}^{-1}$ along with a shift in the zero wind line latitude to south of 20°S.

In the lower stratosphere the early winter period (Figure 7c) now clearly separates the weak vortex years of 2002, 2017, and 2019 by southward shift of the zero wind line location accompanied by EP flux convergence. In the later time period (Figure 7d), we find the years overall much more scattered, with no clear distinction of the weak vortex events.

Finally, we examined if the early winter zero wind line at 1 hPa could be used to identify the SSW years based on the August–September EP flux divergence in the lower stratosphere. Figures 7e)-f) show the EP flux divergence averaged for the time period of 10 August–6 September, while the zero wind line time period remains consistent with the previous panels. We can now see that the years 2002 and 2019 have a very close resemblance to the early winter in the upper stratosphere (Figure 7a), being clearly separated from the other years both in the zero wind line location and the wave momentum deposition. This is not the case for the weak vortex year of 2017, however. Kwon et al. (2020) report the 2017 vortex weakening onset date as August 22. We proceeded to test delayed time periods for the EP flux divergence, but these did not indicate change beyond the roughly -1 $\mathrm{ms}^{-1}\mathrm{day}^{-1}$ range for the year 2017.

We also tested the used of the 10 hPa zero wind line location to see if a measure of the eQBO wind pattern horizontal extent would provide similar results (not shown). As could be expected from Figure 6, this was unsuccessful and the years were simply separated by the difference in EP flux divergence (identical to Figure 7 separation on the y-axis).

While the EP flux convergence, particularly in the upper stratosphere, in early winter would on its own provide some predictability for later conditions, the zero wind line location at 1 hPa appears to add additional separation, particularly when used for the lower stratospheric EP flux divergence (Figure 7c).

4 Discussion

The sudden stratospheric warmings over Antarctica in 2002 and 2019 both have an early winter equatorial SAO-QBO-like wind pattern interaction and coinciding easterly momentum deposition in the polar atmosphere, as indicated by the EP flux convergence. For both years the SAO is presents as a feature of easterly winds (of over 10 ms^{-1}) extending into the SH from early winter. Change in the latitudinal location where winds shift from westerly to easterly influences the waveguide in the upper stratosphere-lower mesosphere, resulting in easterly momentum being deposited on the equatorward side of the polar vortex from early winter. When the QBO and SAO easterly wind features merge, they generate a zero wind line that stretches from the lower stratosphere into the mesosphere ($\sim$30 hPa to 0.3 hPa) near 30°S latitude, now modulating the wave guide across the whole vertical range. This feature continues to be extended towards the pole into August, with continued easterly momentum deposition in the polar atmosphere, decelerating the prevailing westerlies on the equatorward side of the polar vortex. In 2002, the zonal mean zonal winds between about 40°S-60°S decelerate down to below 10 hPa, eventually triggering major SSW conditions. In contrast, in 2019, the zonal mean zonal wind reversal is less focused, taking place across a wider range of latitudes, and major SSW conditions are not fulfilled. In our zonal mean analysis, this suggests that vertical wave propagation from the source regions at high and mid-latitudes is significantly affected, with the movement of the zero wind line creating a barrier for wave propagation.

We found that the weak vortex years of 1988 and 2017 show a similar SAO-QBO wind pattern like merging in July. However, neither of these years show a poleward shift in the zero wind line location as early as was seen for 2002 and 2019. Causes of these differences could be investigated further in a detailed study. We note that in 2017, the changes in dynamics were enough to stifle the growth of the ozone hole (Klekociuk et al., 2020). Our analysis of all other years with similar background QBO conditions in MERRA-2 did not reveal similar behaviour with early winter sustained momentum deposition and similar merging of SAO-QBO-like easterly wind patterns in early winter.

Recently, Gray et al. (2020) reported that in order to accurately predict NH SSWs in an atmospheric model, it was necessary to constrain the model's global tropospheric winds and temperatures, and to further constrain the zonal wind in the equatorial atmosphere above 5 hPa to reanalysis fields. These model results further emphasize those of Gray (2003) who showed similar results for a middle atmosphere only model: that the high altitude equatorial atmosphere plays an important role in NH SSWs. Although our analysis focuses on the SH SSWs in 2002 and 2019, our results present a possible mechanism for this connection. The early winter equatorial SAO-QBO wind pattern interaction with the simultaneous EP flux convergence, and subsequent modulation of the waveguide, reflects mid-latitude waves up and pole-ward, resulting in deceleration of the equatorward side of the polar vortex above 100 hPa. The SAO-QBO-like interaction was not unique to 2019 and 2002 and was found to happen during other easterly QBO years. However the early timing and extent of the zero wind line polerward shift did not occur in these other years. Our results suggest that this may be a reflection of variations not only in QBO, but also in the amplitude and descent of the SAO, the latter of which, to our knowledge, are not well understood (see e.g. Moss et al., 2016; Kawatani et al., 2020). While we focused particularly in scarce SH SSW/weak vortex events here, the the seasonal evolution of the SH

polar vortex and predictability of related climate patterns has been investigated for example by Lim et al. (2018) and Byrne and Shepherd (2018).

We propose that this early winter behaviour may aid in identifying conditions that lead to deceleration of the polar winds, which could then precondition the atmosphere for a SSW. For example in 2019, when there was enhanced upwards wave flux in August (Shen et al., 2020), the modulated waveguide in the stratosphere and above may have provided further optimal conditions for large disturbance to take place. It may also partially explain why SSWs are less common in the Southern Hemisphere: if the early and large SAO-QBO-like merging contributes to optimal conditions for SSW, not only is this dependent the QBO being in the correct phase, but also the SAO having a large amplitude during the early-mid winter. The SH winter typically experiences smaller amplitude SAO easterlies, while the NH winter experiences much larger easterly winds (Smith et al., 2017). However, this hypothesis would need to be tested separately for the NH. It is also important to note again that the NH has higher winter planetary wave activity and variability than the SH.

As we find that these early patterns start occurring 2-3 months before the SSW or vortex weakening events, the behaviour of the equatorial middle atmosphere along with the polar response at this stage may signal an imminent SSW event, potentially providing predictability beyond the typical 10-15 day window in SSW prediction in the NH (Domeisen et al., 2020), with some signals possibly appearing as early as 30 days in advance (Lawrence and Manney, 2020). As reported by Rao et al. (2020c), for the 2019 SH minor SSW, the predictive limit from forecast models was 18 days. The results reported here could potentially aid subseasonal to seasonal (S2S) prediction (Domeisen et al., 2019a, 2020). However, as the motivation for this study was to better understand early signals for the 2019 SH event, this will need to be tested in detail for the NH atmosphere first. We note that the results presented by Gray et al. (2020) (their Figures 3-4) suggest that coupling of the SAO and QBO zonal wind patterns, similar to our SH cases, took place in their simulation approximately 2 months before the onset of the NH January 2009 SSW. As noted by Gray et al. (2020), the atmospheric region where the SAO originates (mesosphere), tends to be neglected in model development. Our results provide further evidence that these altitudes are not only important for understanding the NH but also the SH extreme dynamical events. As noted by the multi-model study of Rao et al. (2020b), representation of the QBO is also remains a challenge.

As mentioned earlier, much work has been done in understanding both causes and implications of SSWs, particularly in the NH. Many interactions with large scale atmospheric modes or external forcing have been found to influence NH SSW occurrence, including the QBO, the ENSO, solar cycle, and the MJO. Due to the scarcity of SH SSW events we were unable to investigate the potential individual influences of these. However, we note that ENSO conditions, based on the Multivariate ENSO Index (MEI.v2, Zhang et al. (2019); Multivariate ENSO Index Version 2 (MEI.v2)), were neutral, while the MJO index amplitude (Wheeler and Hendon, 2004; Madden–Julian oscillation index (MJO)) was positive, during both 2002 and 2019. Note that the MJO index amplitude corresponds to $\sqrt{\mathrm{RMM1}^2 + \mathrm{RMM2}^2}$, as defined by Wheeler and Hendon (2004), and does not account for the MJO phase. For the weak vortex years of 1988 and 2017 the MJO was generally variable during the austral winter, while the ENSO index was negative, and thus opposite to the two generally recognised SSW years. These differences could signal the importance of teleconnections in the SH polar responses.

5 Conclusions

Sudden stratospheric warmings are disruptions to the seasonal cycle of the polar winds. Only two well-documented ones have occurred over Antarctica: a major SSW in 2002 and a minor one in 2019, although Kwon et al. (2020) have noted an increasing trend in the number of southern stratospheric polar vortex weakening events in the last two decades. Here we present results based on the MERRA-2 reanalysis, showing that during both years, 2002 and 2019:

1. From early winter, waves are depositing momentum in the equatorward side of the upper-stratospheric–lower mesospheric polar vortex in a manner that is consistent with the equatorial upper stratospheric SAO-like wind structure pushing the waveguide boundary into the SH extratropics.

2. In early winter, SAO and QBO-like wind patterns merge in the equatorial atmosphere, driving further momentum deposition, and thus zonal wind deceleration, in the polar vortex.

3. Changing zonal wind further influences wave propagation conditions, ultimately transferring the signal to the lower stratosphere, likely contributing to favourable propagation conditions for enhanced tropospheric wave forcing later in the winter, resulting in the observed SSWs.

Years 2002, 2019, and the early onset vortex weakening event year of 2017, all depict some of the highest easterly equatorial upper stratospheric SAO zonal mean zonal winds ($U_{1\text{hPa}} < -10$ ms^{-1}) in June. These are accompanied by a significant ($> 2 \times \sigma$) southward shift of the latitudinal location where zonal winds reverse direction from (polar) westerly to (equatorial) easterly. Along with the high amplitude SAO winds, these years also show easterly 10 hPa QBO throughout June (-35 ms$^{-1} < U_{10\text{hPa}} < -20$ ms^{-1}), suggesting that the SAO amplitude alone is not sufficient to understand these SH vortex weakening events, but the QBO phase in early winter also plays a role.

Previous work focused on the more frequent NH SSWs has pointed to the role of the equatorial upper stratosphere and mesosphere particularly when predicting the timings of NH SSW (Gray et al., 2020). Our analysis of the two SH SSWs suggest that, at least for the Southern Hemisphere, the merging of the eQBO and the SAO-like wind patterns in the equatorial upper stratosphere-mesosphere seems critical in triggering the polar disturbances. The wind pattern in 2002 and 2019 is not unique, however, this occurs much earlier in the season than other easterly QBO years, leading to early winter deposition of momentum, as indicated by the EP flux divergence, that decelerates the winds in the equatorward side of the polar vortex by -3 to -2.5 ms^{-1}day^{-1} from mid-June onwards.

When considering the early winter EP flux divergence together with the latitudinal location of the zero wind line at 1 hPa, we were able to identify the SSW/early onset vortex weakening event years up to 60 days before the events. We postulate that this early winter behaviour may be a key physical process in decelerating the polar vortex winds, leading to preconditioning of the polar atmosphere for a SSW. The occurrence of these patterns in the equatorial atmosphere and in the polar upper atmosphere during early winter could provide extended predictability of SSWs from the typical 10-18 day window (Domeisen et al., 2020; Lawrence and Manney, 2020; Rao et al., 2020c).

As our present analysis is focused on events that took place in the SH, further work would be needed to test to what extent these SAO-QBO-like patterns might play a role in NH SSWs. This future work may help shed light on the different roles background flow and wave enhancement have on triggering the SH and NH SSWs, which may help explain why SH SSWs occur less frequently than NH SSWs.

Data availability. The MERRA-2 dataset is freely available (see Global Modeling and Assimilation Office (GMAO), 2015).
The ENSO Index, MEI.v2 (Zhang et al., 2019) is freely available (see Multivariate ENSO Index Version 2 (MEI.v2)).
The MJO index (Wheeler and Hendon, 2004) is freely available (see Madden–Julian oscillation index (MJO)).

Author contributions. AS and VJN planned the study, analysed the MERRA-2 data and contributed to the writing of the article.

Competing interests. The authors declare no competing interests.

Acknowledgements. We are grateful for the open access to the MERRA-2 reanalysis data products provided by GES DISC.
The work of VJN was supported by a postgraduate scholarship provided by the University of Otago Physics Department.

References

Albers, J. R. and Birner, T.: Vortex Preconditioning due to Planetary and Gravity Waves prior to Sudden Stratospheric Warmings, Journal of the Atmospheric Sciences, 71, 4028–4054, https://doi.org/10.1175/jas-d-14-0026.1, 2014.

Allen, D. R., Bevilacqua, R. M., Nedoluha, G. E., Randall, C. E., and Manney, G. L.: Unusual stratospheric transport and mixing during the 2002 Antarctic winter, Geophysical Research Letters, 30, 1599, https://doi.org/10.1029/2003GL017117, 2003.

Anstey, J. A. and Shepherd, T. G.: High-latitude influence of the quasi-biennial oscillation, Quarterly Journal of the Royal Meteorological Society, 140, 1–21, https://doi.org/10.1002/qj.2132, 2014.

Baldwin, M. P. and Dunkerton, T. J.: Stratospheric Harbingers of Anomalous Weather Regimes, Science, 294, 581–584, https://doi.org/10.1126/science.1063315, 2001.

Baldwin, M. P., Gray, L. J., Dunkerton, T. J., Hamilton, K., Haynes, P. H., Randel, W. J., Holton, J. R., Alexander, M. J., Hirota, I., Horinouchi, T., Jones, D. B. A., Kinnersley, J. S., Marquardt, C., Sato, K., and Takahashi, M.: The quasi-biennial oscillation, Rev. Geophys., 39, 179 – 229, https://doi.org/10.1029/1999RG000073, 2001.

Baldwin, M. P., Ayarzagüena, B., Birner, T., Butchart, N., Butler, A. H., Charlton-Perez, A. J., Domeisen, D. I. V., Garfinkel, C. I., Garny, H., Gerber, E. P., Hegglin, M. I., Langematz, U., and Pedatella, N. M.: Sudden Stratospheric Warmings, Reviews of Geophysics, 59, e2020RG000 708, https://doi.org/10.1029/2020RG000708, 2021.

Bosilovich, M. G., Lucchesi, R., and Suarez, M.: 2016: MERRA-2: File Specification. GMAO Office Note No. 9 (Version 1.1), Tech. rep., Global Modeling and Assimilation Office Earth Sciences Division NASA Goddard Space Flight Center, Greenbelt, Maryland 20771, http://gmao.gsfc.nasa.gov/pubs/office_notes., last accessed 24 Nov, 2020, 2016.

Bracegirdle, T. J.: The seasonal cycle of stratosphere-troposphere coupling at southern high latitudes associated with the semi-annual oscillation in sea-level pressure, Clim. Dyn., 37, 2323–2333, https://doi.org/10.1007/s00382-011-1014-4, 2011.

Byrne, N. J. and Shepherd, T. G.: Seasonal persistence of circulation anomalies in the Southern Hemisphere stratosphere, and its implications for the troposphere, Journal of Climate, 31, 3467–3483, https://doi.org/10.1175/jcli-d-17-0557.1, 2018.

Charlton, A. J. and Polvani, L. M.: A New Look at Stratospheric Sudden Warmings. Part I: Climatology and Modeling Benchmarks, J. Clim., 20, 449–469, https://doi.org/10.1175/JCLI3996.1, 2007.

Coy, L., Wargan, K., Molod, A. M., McCarty, W. R., and Pawson, S.: Structure and Dynamics of the Quasi-Biennial Oscillation in MERRA-2, J. Clim., 29, 5339–5354, https://doi.org/10.1175/JCLI-D-15-0809.1, https://doi.org/10.1175/JCLI-D-15-0809.1, 2016.

de la Cámara, A., Birner, T., and Albers, J. R.: Are Sudden Stratospheric Warmings Preceded by Anomalous Tropospheric Wave Activity?, Journal of Climate, 32, 7173 – 7189, https://doi.org/10.1175/jcli-d-19-0269.1, 2019.

Doddridge, E. W. and Marshall, J.: Modulation of the Seasonal Cycle of Antarctic Sea Ice Extent Related to the Southern Annular Mode, Geophys. Res. Lett., 44, 9761–9768, https://doi.org/10.1002/2017GL074319, 2017.

Domeisen, D. I. V., Butler, A. H., Perez, A. J. C., Ayarzagüena, B., Baldwin, M. P., Sigouin, E. D., Furtado, J. C., Garfinkel, C. I., Hitchcock, P., Karpechko, A. Y., Kim, H., Knight, J. R., Lang, A. L., Lim, E. P., Marshall, A., Roff, G., Schwartz, C., Simpson, I. R., Son, S.-W., and Taguchi, M.: The role of the stratosphere in subseasonal to seasonal prediction Part II: Predictability arising from stratosphere - troposphere coupling, J. Geophys. Res.: Atmos., 125, 2019JD030 923, https://doi.org/10.1029/2019JD030923, 2019a.

Domeisen, D. I. V., Garfinkel, C. I., and Butler, A. H.: The Teleconnection of El Niño Southern Oscillation to the Stratosphere, Rev. Geophys., 57, 5–47, https://doi.org/10.1029/2018RG000596, 2019b.

Domeisen, D. I. V., Butler, A. H., Perez, A. J. C., Ayarzagüena, B., Baldwin, M. P., Sigouin, E. D., Furtado, J. C., Garfinkel, C. I., Hitchcock, P., Karpechko, A. Y., Kim, H., Knight, J. R., Lang, A. L., Lim, E. P., Marshall, A., Roff, G., Schwartz, C., Simpson, I. R., Son, S.-W., and Taguchi, M.: The Role of the Stratosphere in Subseasonal to Seasonal Prediction: 1. Predictability of the Stratosphere, Journal of Geophysical Research: Atmospheres, 125, e2019JD030 920, https://doi.org/10.1029/2019jd030920, 2020.

Edmon, H. J., Hoskins, B. J., and McIntyre, M. E.: Eliassen-Palm Cross Sections for the Troposphere, J. Atmos. Sci., 37, 2600 – 2616, 1980.

Eswaraiah, S., Kim, Y. H., Hong, J., Kim, J.-H., Ratnam, M. V., Chandran, A., Rao, S., and Riggin, D.: Mesospheric signatures observed during 2010 minor stratospheric warming at King Sejong Station (62 °S, 59 °W), J. Atmos. Sol.-Ter. Phys., 140, 55 – 64, https://doi.org/10.1016/j.jastp.2016.02.007, 2016.

Eswaraiah, S., Kim, Y. H., Lee, J., Ratnam, M. V., and Rao, S. V. B.: Effect of Southern Hemisphere Sudden Stratospheric Warmings on Antarctica Mesospheric Tides: First Observational Study, J. Geophys. Res.: Space Physics, 123, 2127–2140, https://doi.org/10.1002/2017JA024839, 2018.

Eswaraiah, S., Kim, J.-H., Lee, W., Hwang, J., Kumar, K. N., and Kim, Y. H.: Unusual Changes in the Antarctic Middle Atmosphere During the 2019 Warming in the Southern Hemisphere, Geophys. Res. Lett., 47, e2020GL089 199, https://doi.org/10.1029/2020GL089199, 2020a.

Eswaraiah, S., Lee, C., Lee, W., Kim, Y. H., Kumar, K. N., and Medineni, V. R.: Temperature tele-connections between the tropical and polar middle atmosphere in the Southern Hemisphere during the 2010 minor sudden stratospheric warming, Atmospheric Science Letters, 22, e1010, https://doi.org/10.1002/asl.1010, 2020b.

Garcia, R. R., Dunkerton, T. J., Lieberman, R. S., and Vincent, R. A.: Climatology of the semiannual oscillation of the tropical middle atmosphere, J. Geophys. Res.: Atmos., 102, 26 019–26 032, https://doi.org/10.1029/97JD00207, 1997.

Gelaro, R., McCarty, W., Suárez, M. J., Todling, R., Molod, A., Takacs, L., Randles, C. A., Darmenov, A., Bosilovich, M. G., Reichle, R., Wargan, K., Coy, L., Cullather, R., Draper, C., Akella, S., Buchard, V., Conaty, A., Silva, A. M. D., Gu, W., Kim, G.-K., Koster, R., Lucchesi, R., Merkova, D., Nielsen, J. E., Partyka, G., Pawson, S., Putman, W., Rienecker, M., Schubert, S. D., Sienkiewicz, M., and Zhao, B.: The Modern-Era Retrospective Analysis for Research and Applications, Version 2 (MERRA-2), J. Clim., pp. 5419–5454, 2017.

Global Modeling and Assimilation Office (GMAO): MERRA-2 inst6_3d_ana_Np: 3d,6-Hourly,Instantaneous,Pressure-Level,Analysis,Analyzed Meteorological Fields V5.12.4, Greenbelt, MD, USA, Goddard Earth Sciences Data and Information Services Center (GES DISC), 10.5067/A7S6XP56VZWS, doi:0.5067/A7S6XP56VZWS, accessed 21 October 2020, 2015.

Gray, L.: The influence of the equatorial upper stratosphere on stratospheric sudden warmings, Geophys. Res. Lett., 30, 1166, https://doi.org/10.1029/2002GL016430, 2003.

Gray, L. J., Brown, M. J., Knight, J., Andrews, M., Lu, H., O'Reilly, C., and Anstey, J.: Forecasting extreme stratospheric polar vortex events, Nature Comm., 11, https://doi.org/10.1038/s41467-020-18299-7, 2020.

Holton, J. R. and Tan, H.-C.: The Influence of the Equatorial Quasi-Biennial Oscillation on the Global Circulation at 50 mb, J. Atmos. Sci., 37, 2200–2208, https://doi.org/10.1175/1520-0469(1980)037<2200:TIOTEQ>2.0.CO;2, 1980.

Hoppel, K., Bevilacqua, R., Allen, D., Nedoluha, G., and Randall, C.: POAM III observations of the anomalous 2002 Antarctic ozone hole, Geophys. Res. Lett., 30, 1394, https://doi.org/10.1029/2003GL016899, 2003.

Kanzawa, H. and Kawaguchi, S.: Large stratospheric sudden warming in Antarctic late winter and shallow ozone hole in 1988, Geophysical Research Letters, 17, 77–80, https://doi.org/10.1029/GL017i001p00077, 1990.

Kawatani, Y., Hirooka, T., Hamilton, K., Smith, A. K., and Fujiwara, M.: Representation of the equatorial stratopause semiannual oscillation in global atmospheric reanalyses, Atmos. Chem. Phys., 20, 9115–9133, https://doi.org/10.5194/acp-20-9115-2020, 2020.

Klekociuk, A., Tully, M., Krummel, P., Kravchenko, V., Henderson, S., Alexander, S., Querel, R., Nichol, S., Smale, D., Milinevsky, G., Grytsai, A., Fraser, P., Xiangdong, Z., Gies, H., Schofield, R., and Shanklin, J.: The Antarctic ozone hole during 2017, Journal of Southern Hemisphere Earth Systems Science, 69, 29–51, https://doi.org/10.1071/ES19019, 2020.

Kuai, L., Shia, R.-L., Jiang, X., Tung, K. K., and Yung, Y. L.: Nonstationary Synchronization of Equatorial QBO with SAO in Observations and a Model, J. Atmos. Sci., 66, 1654–1664, https://doi.org/10.1175/2008JAS2857.1, 2009.

Kwon, H., Choi, H., Kim, B.-M., Kim, S.-W., and Kim, S.-J.: Recent weakening of the southern stratospheric polar vortex and its impact on the surface climate over Antarctica, Environmental Research Letters, 15, 094 072, https://doi.org/10.1088/1748-9326/ab9d3d, 2020.

Labitzke, K.: On the solar cycle–QBO relationship: a summary, J. Atmos. Sol. Terr. Phys., 67, 45–54, https://doi.org/10.1016/j.jastp.2004.07.016, 2005.

Lawrence, Z. D. and Manney, G. L.: Does the Arctic Stratospheric Polar Vortex Exhibit Signs of Preconditioning Prior to Sudden Stratospheric Warmings?, J. Atmos. Sci., 77, 611–632, https://doi.org/10.1175/JAS-D-19-0168.1, 2020.

Lim, E.-P., Hendon, H. H., and Thompson, D. W. J.: Seasonal Evolution of Stratosphere-Troposphere Coupling in the Southern Hemisphere and Implications for the Predictability of Surface Climate, Journal of Geophysical Research: Atmospheres, 123, 12,002–12,016, https://doi.org/10.1029/2018JD029321, 2018.

Lim, E. P., Hendon, H. H., Boschat, G., Hudson, D., Thompson, D. W. J., Dowdy, A. J., and Arblaster, J. M.: Australian hot and dry extremes induced by weakenings of the stratospheric polar vortex, Nature Geosci., 12, 896–901, https://doi.org/10.1038/s41561-019-0456-x, 2019.

Madden–Julian oscillation index (MJO): https://www.cpc.ncep.noaa.gov/products/precip/CWlink/MJO/whindex.shtml, last accessed 24 May, 2021.

Matsuno, T.: A Dynamical Model of the Stratospheric Sudden Warming, Journal of Atmospheric Sciences, 28, 1479–1494, https://doi.org/10.1175/1520-0469(1971)028<1479:ADMOTS>2.0.CO;2, 1971.

Moss, A. C., Wright, C. J., Davis, R. N., and Mitchell, N. J.: Gravity-wave momentum fluxes in the mesosphere over Ascension Island (8°S, 14°W) and the anomalous zonal winds of the semi-annual oscillation in 2002, Ann. Geophys., 34, 323–330, https://doi.org/10.5194/angeo-34-323-2016, 2016.

Multivariate ENSO Index Version 2 (MEI.v2): https://psl.noaa.gov/enso/mei/, last accessed 3 Dec, 2020.

Pascoe, C. L., Gray, L. J., and Scaife, A. A.: A GCM study of the influence of equatorial winds on the timing of sudden stratospheric warmings, Geophys. Res. Lett., 33, L06 825, https://doi.org/10.1029/2005GL024715, 2006.

Peña-Ortiz, C., Schmidt, H., Giorgetta, M. A., and Keller, M.: QBO modulation of the semiannual oscillation in MAECHAM5 and HAMMONIA, J. Geophys. Res.: Atmos., 115, D21 106, https://doi.org/10.1029/2010JD013898, 2010.

Rao, J., Garfinkel, C. I., Chen, H., and White, I. P.: The 2019 New Year Stratospheric Sudden Warming and Its Real-Time Predictions in Multiple S2S Models, Journal of Geophysical Research: Atmospheres, 124, 11 155–11 174, https://doi.org/10.1029/2019jd030826, 2019.

Rao, J., Garfinkel, C. I., and White, I. P.: Predicting the Downward and Surface Influence of the February 2018 and January 2019 Sudden Stratospheric Warming Events in Subseasonal to Seasonal (S2S) Models, Journal of Geophysical Research: Atmospheres, 125, e2019JD031 919, https://doi.org/10.1029/2019jd031919, 2020a.

Rao, J., Garfinkel, C. I., and White, I. P.: How does the Quasi- Biennial Oscillation affect the boreal winter tropospheric circulation in CMIP5/6 models?, Journal of Climate, 33, 1–54, https://doi.org/10.1175/jcli-d-20-0024.1, 2020b.

Rao, J., Garfinkel, C. I., White, I. P., and Schwartz, C.: The Southern Hemisphere Minor Sudden Stratospheric Warming in September 2019 and its Predictions in S2S Models, J. Geophys. Res.: Atmos., 125, e2020JD032 723, https://doi.org/10.1029/2020JD032723, 2020c.

Ricaud, P., Lefèvre, F., Berthet, G., Murtagh, D., Llewellyn, E. J., Mégie, G., Kyrölä, E., Leppelmeier, G. W., Auvinen, H., Boonne, C., Brohede, S., Degenstein, D. A., de La Noë, J., Dupuy, E., El Amraoui, L., Eriksson, P., Evans, W. F. J., Frisk, U., Gattinger, R. L., Girod, F., Haley, C. S., Hassinen, S., Hauchecorne, A., Jimenez, C., Kyrö, E., Lautié, N., Le Flochmoën, E., Lloyd, N. D., McConnell, J. C., McDade, I. C., Nordh, L., Olberg, M., Pazmino, A., Petelina, S. V., Sandqvist, A., Seppälä, A., Sioris, C. E., Solheim, B. H., Stegman, J., Strong, K., Taalas, P., Urban, J., von Savigny, C., von Scheele, F., and Witt, G.: Polar vortex evolution during the 2002 Antarctic major warming as observed by the Odin satellite, J. Geophys. Res.: Atmos., 110, D05 302, https://doi.org/10.1029/2004JD005018, 2005.

Richter, J. H., Matthes, K., Calvo, N., and Gray, L. J.: Influence of the quasi-biennial oscillation and El Niño–Southern Oscillation on the frequency of sudden stratospheric warmings, J. Geophys. Res.: Atmos., 116, D20 111, https://doi.org/10.1029/2011JD015757, 2011.

Schoeberl, M. R., Stolarski, R. S., and Krueger, A. J.: The 1988 Antarctic ozone depletion: Comparison with previous year depletions, Geophysical Research Letters, 16, 377–380, https://doi.org/https://doi.org/10.1029/GL016i005p00377, 1989.

Schwartz, C. and Garfinkel, C. I.: Relative roles of the MJO and stratospheric variability in North Atlantic and European winter climate, Journal of Geophysical Research: Atmospheres, 122, 4184–4201, https://doi.org/10.1002/2016JD025829, 2017.

Shen, X., Wang, L., and Osprey, S.: The Southern Hemisphere sudden stratospheric warming of September 2019, Science Bulletin, 65, 1800–1802, https://doi.org/10.1016/j.scib.2020.06.028, 2020.

Smith, A. K., Garcia, R. R., Moss, A. C., and Mitchell, N. J.: The Semiannual Oscillation of the Tropical Zonal Wind in the Middle Atmosphere Derived from Satellite Geopotential Height Retrievals, Journal of the Atmospheric Sciences, 74, 2413–2425, https://doi.org/10.1175/jas-d-17-0067.1, 2017.

Smith, A. K., Holt, L. A., Garcia, R. R., Anstey, J. A., Serva, F., Butchart, N., Osprey, S., Bushell, A. C., Kawatani, Y., Kim, Y.-H., Lott, F., Braesicke, P., Cagnazzo, C., Chen, C.-C., Chun, H.-Y., Gray, L., Kerzenmacher, T., Naoe, H., Richter, J., Versick, S., Schenzinger, V., Watanabe, S., and Yoshida, K.: The equatorial stratospheric semiannual oscillation and time-mean winds in QBOi models, Q. J. R. Meteorol. Soc., pp. 1–17, https://doi.org/10.1002/qj.3690, 2020.

Solomon, S.: Stratospheric ozone depletion: A review of concepts and history, Rev. Geophys., 37, 275–316, https://doi.org/10.1029/1999RG900008, 1999.

Solomon, S., Garcia, R. R., Rowland, F. S., and Wuebbles, D. J.: On the depletion of Antarctic ozone, Nature, 321, 755–758, https://doi.org/10.1038/321755a0, 1986.

Taguchi, M. and Hartmann, D. L.: Interference of extratropical surface climate anomalies induced by El Niño and stratospheric sudden warmings, Geophys. Res. Lett., 32, L04 709, https://doi.org/10.1029/2004GL022004, 2005.

Thompson, D. W. J., Baldwin, M. P., and Solomon, S.: Stratosphere–Troposphere Coupling in the Southern Hemisphere, Journal of the Atmospheric Sciences, 62, 708–715, https://doi.org/10.1175/jas-3321.1, 2005.

Watson, P. A. G. and Gray, L. J.: How does the quasi-biennial oscillation affect the stratospheric polar vortex?, J. Atmos. Sci., 71, 391–409, https://doi.org/10.1175/JAS-D-13-096.1, 2014.

Wheeler, M. C. and Hendon, H. H.: An All-Season Real-Time Multivariate MJO Index: Development of an Index for Monitoring and Prediction, Monthly Weather Review, 132, 1917–1932, https://doi.org/10.1175/1520-0493(2004)132<1917:AARMMI>2.0.CO;2, 2004.

Yamazaki, Y., Matthias, V., Miyoshi, Y., Stolle, C., Siddiqui, T., Kervalishvili, G., Laštovička, J., Kozubek, M., Ward, W., Themens, D. R., Kristoffersen, S., and Alken, P.: September 2019 Antarctic Sudden Stratospheric Warming: Quasi-6-Day Wave Burst and Ionospheric Effects, Geophys. Res. Lett., 47, e2019GL086 577, https://doi.org/10.1029/2019GL086577, 2020.

Zhang, T., Hoell, A., Perlwitz, J., Eischeid, J., Murray, D., Hoerling, M., and Hamill, T. M.: Towards Probabilistic Multivariate ENSO Monitoring, Geophys. Res. Lett., 46, 10 532–10 540, https://doi.org/10.1029/2019GL083946, 2019.

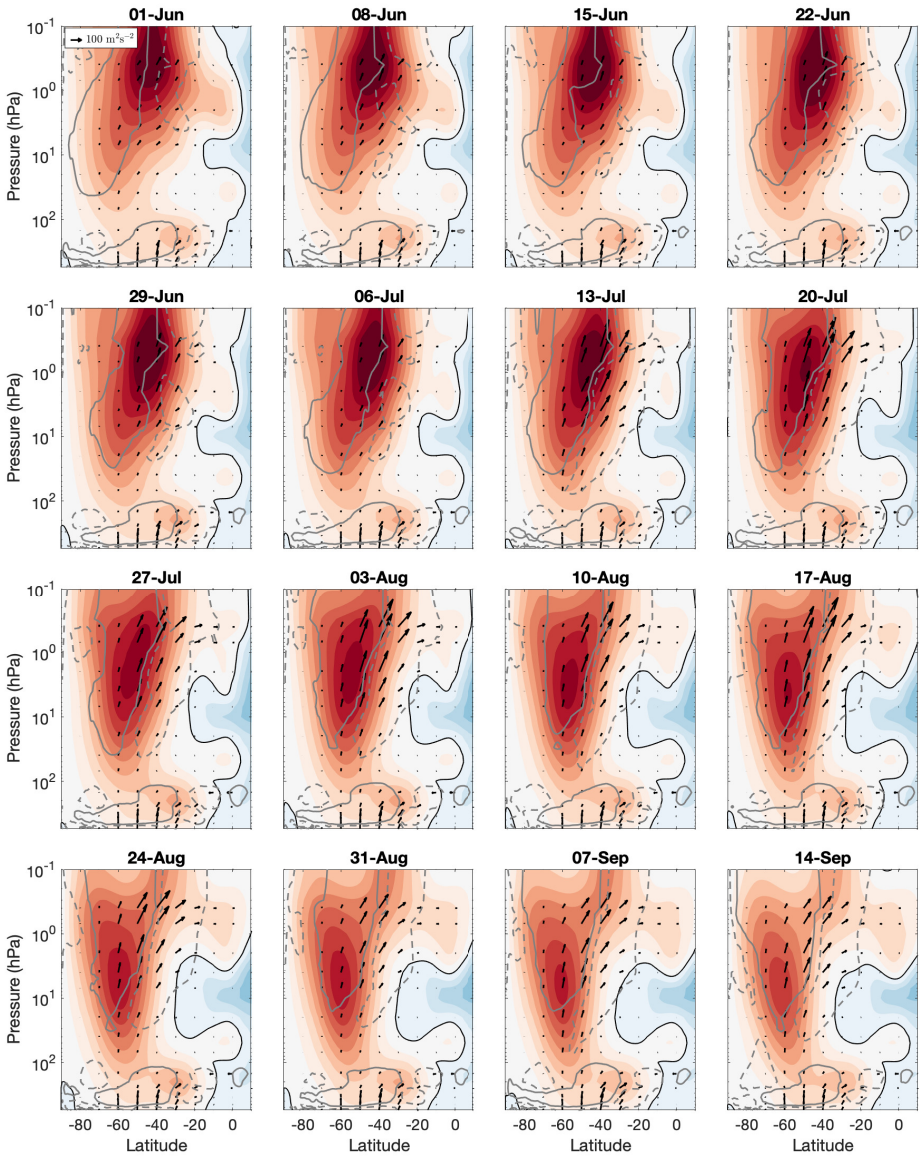

Figure 1. 7-day average zonal mean zonal wind (contours, interval 10 ms^{-1}), Eliassen-Palm (EP) flux (arrows, m^2s^{-2}, reference arrow shown in first panel) and EP flux divergence (± 2 $ms^{-1}day^{-1}$, convergence indicated by dashed grey lines, divergence indicated by solid grey lines) for the reference eQBO years (excluding 1988, 2002, 2017 and 2019). Each figure covers the latitudinal range of 90°S to 10°N and the vertical range of 550 hPa to 0.1 hPa. The solid black line shows the location of the zero wind line. First day of averaging in each figure is given in the title.

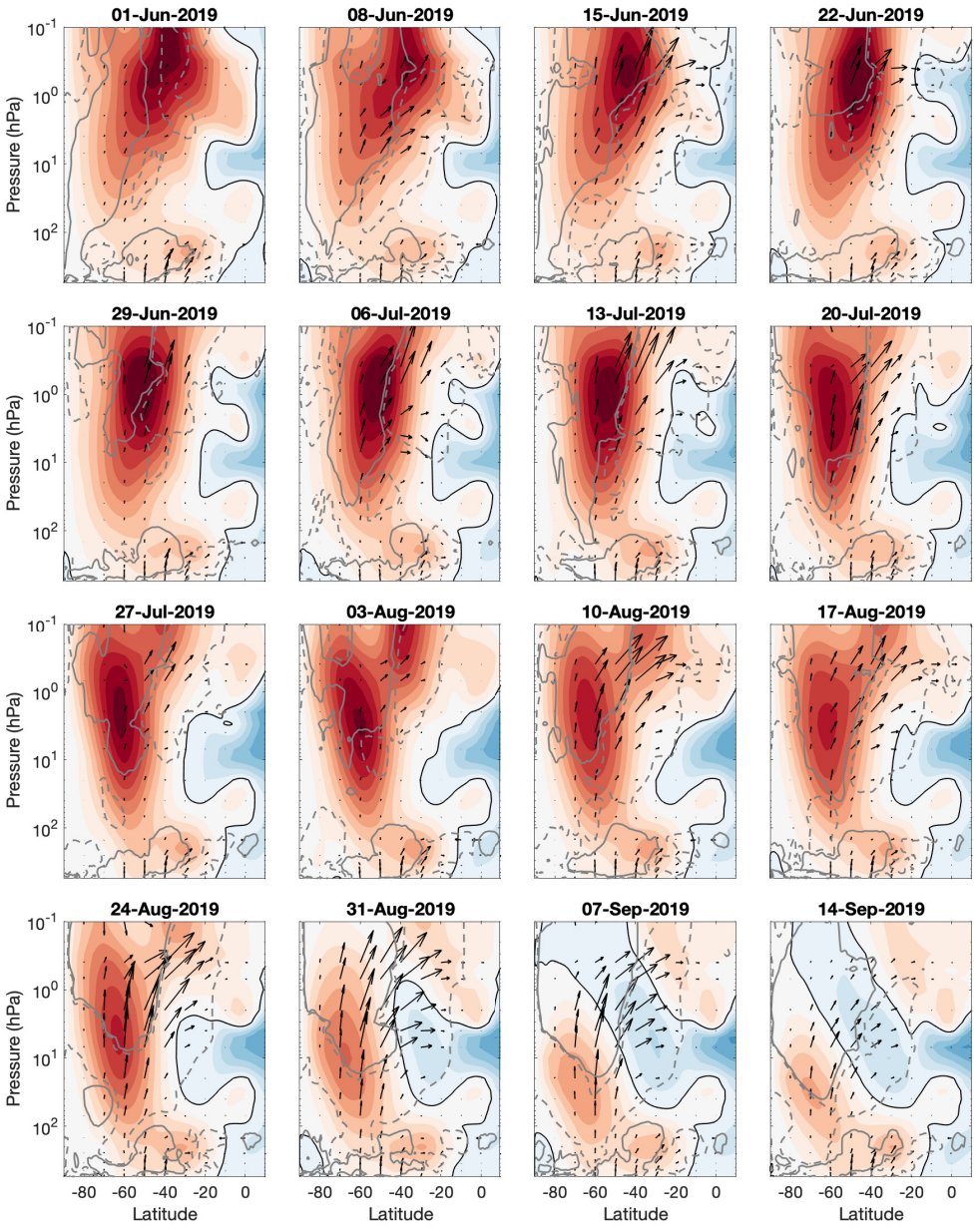

Figure 2. As Figure 1 but for the year 2019.

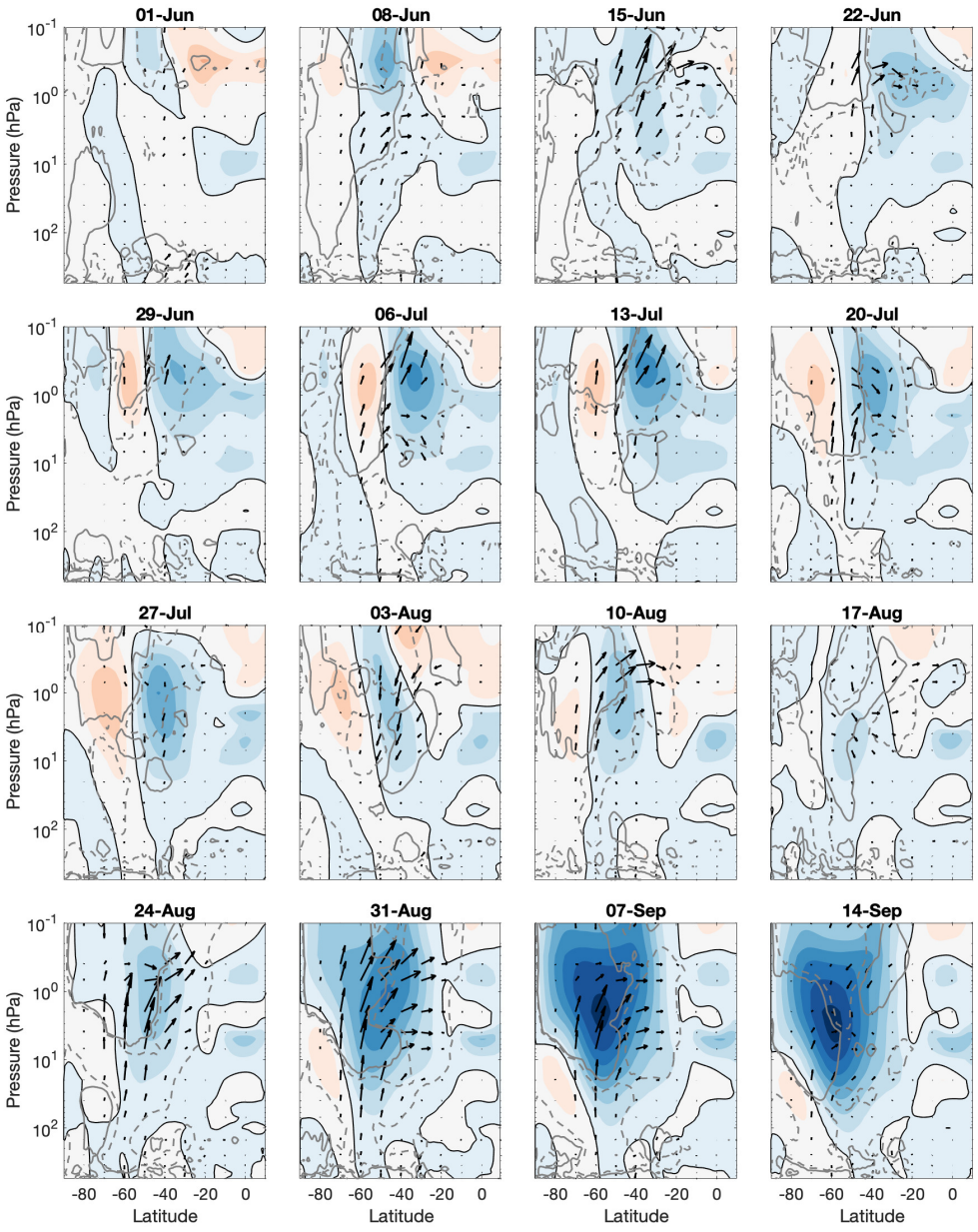

Figure 3. Anomaly: 2019 - reference eQBO years. Zonal wind anomaly contours, EP-flux vectors and divEP levels as in Figure 1.

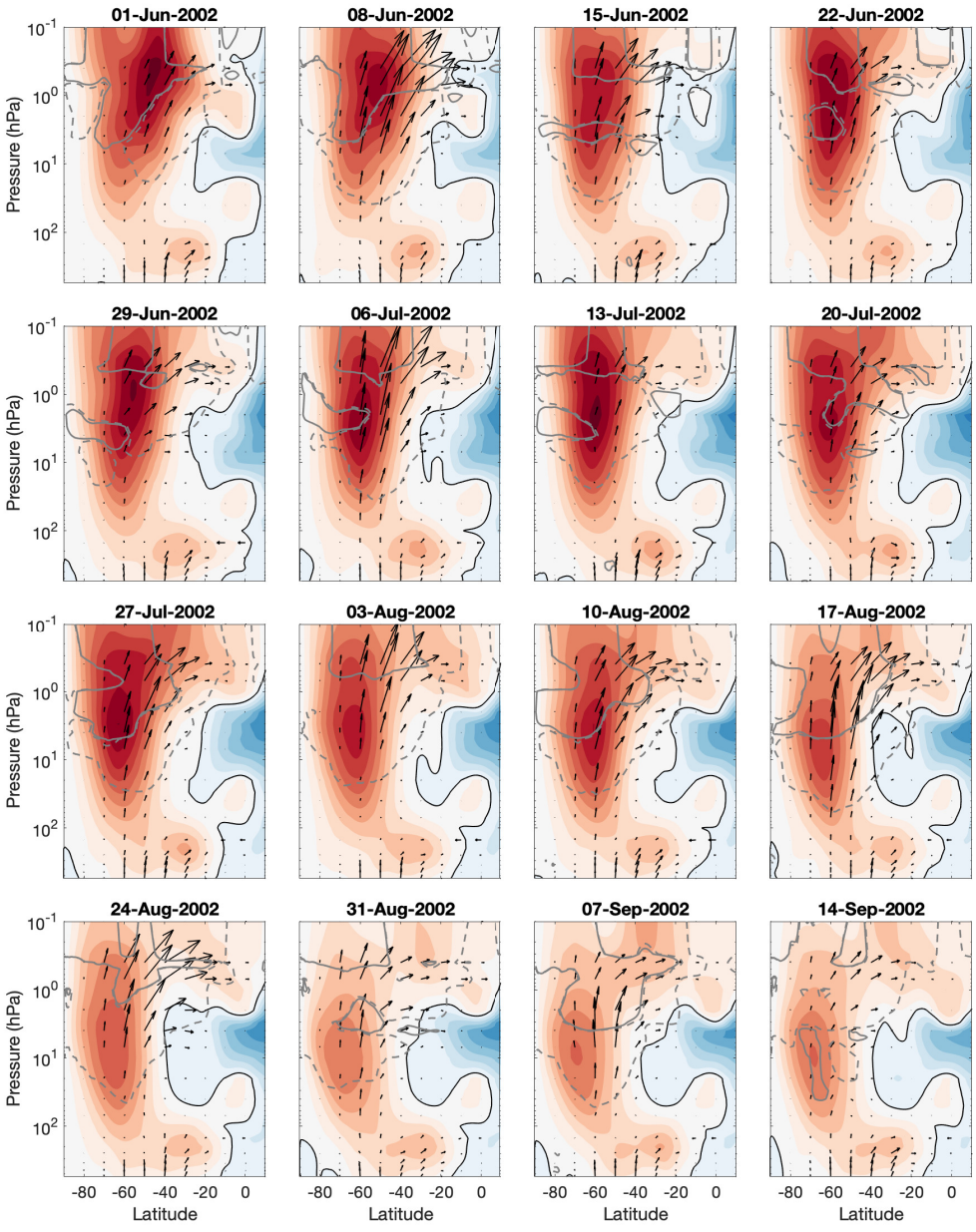

Figure 4. As Figure 1 but for the year 2002.

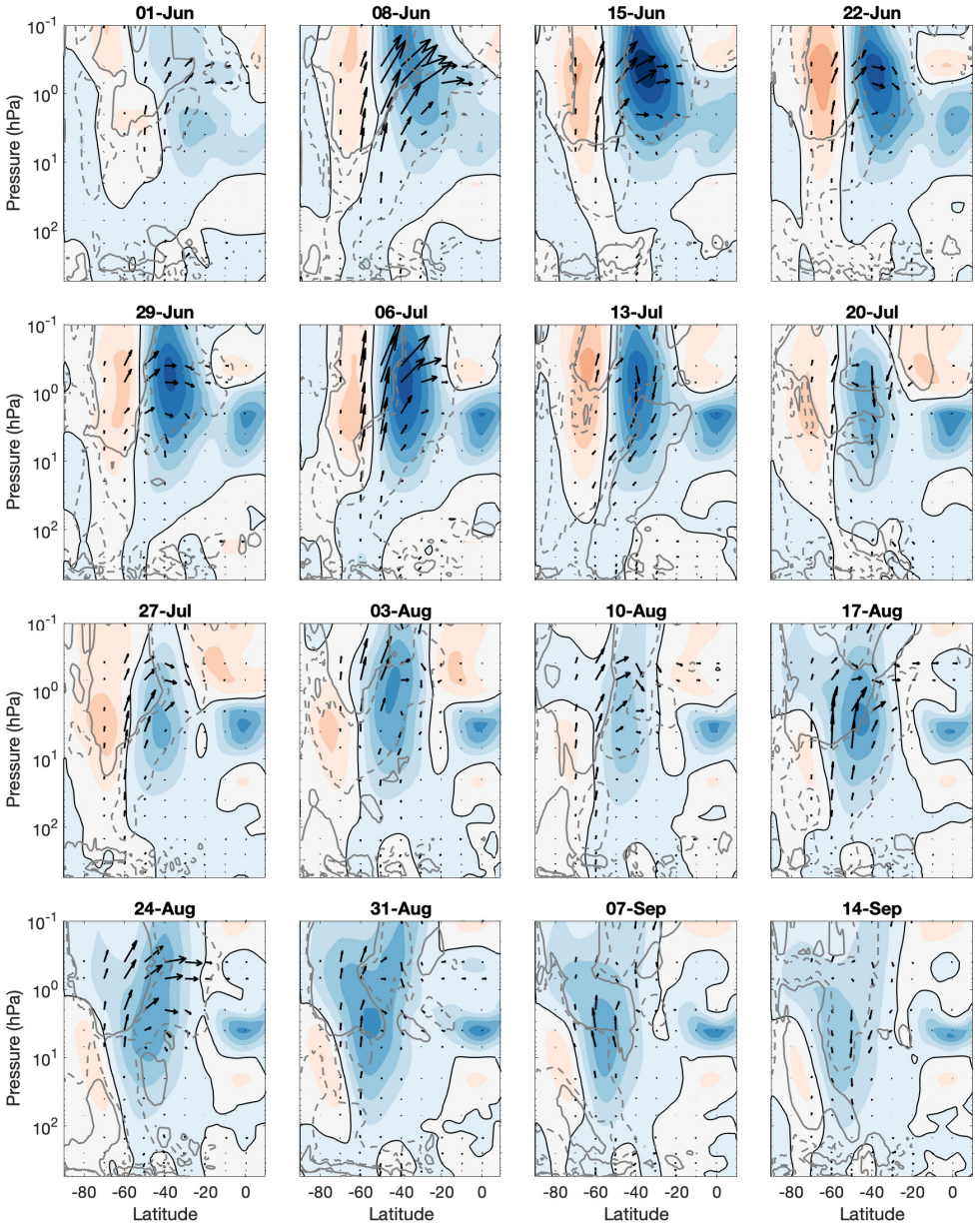

Figure 5. As Figure 3 but now showing the anomaly for the year 2002.

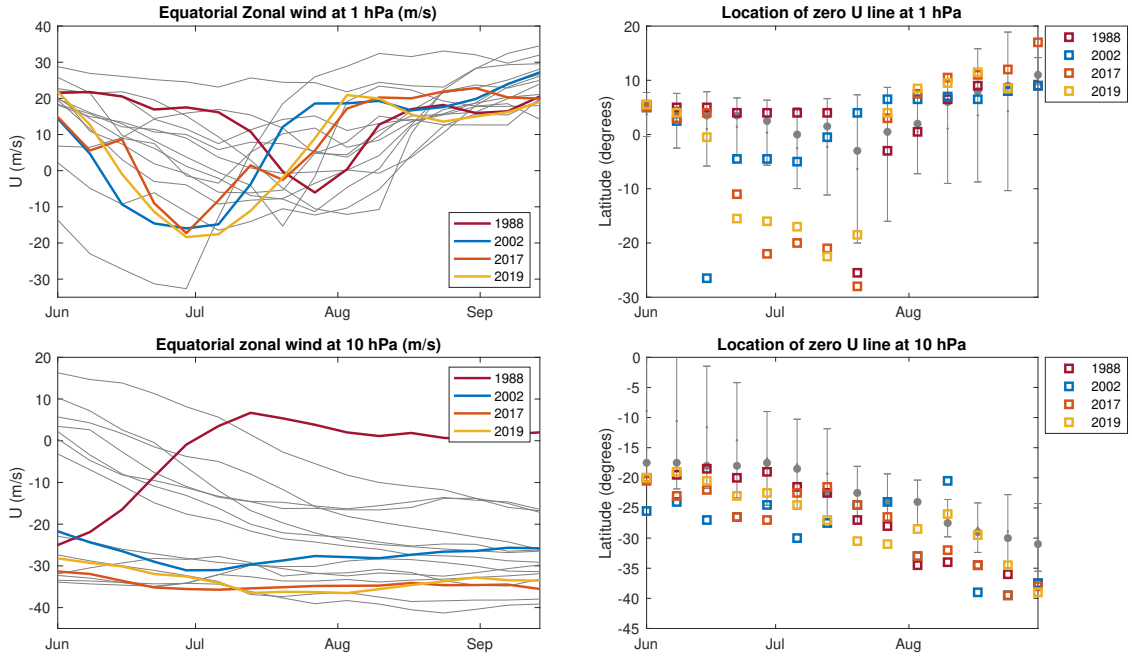

Figure 6. Top (left): Evolution of the equatorial (5°S-5°N) SAO zonal wind at 1 hPa level (ms^{-1}) from June to September. The grey lines show the wind for all eQBO years with the years 1988, 2002, 2017, and 2019 highlighted with red, blue, orange, and yellow lines, respectively. Top (right) Latitudinal location of the zero zonal wind line at 1 hPa level. The small grey dot indicates the mean location while the large grey circle indicates the median location during the eQBO years. For clarity, the grey bars show the $1 \times \sigma$ deviation around the mean location. Years 1988, 2002, 2017, and 2019 are highlighted with red, blue, orange, and yellow markers, respectively. Bottom: As above, but for the zonal wind at the 10 hPa level for QBO.

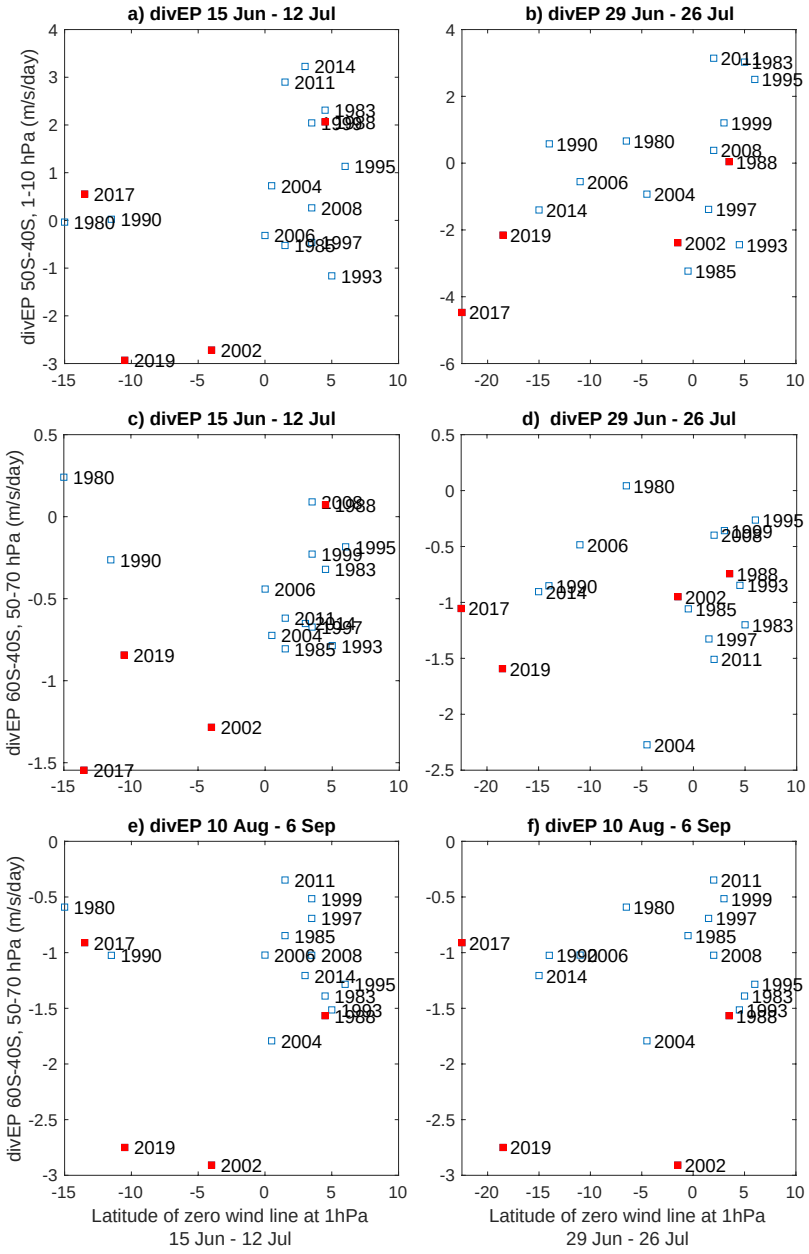

Figure 7. Latitude of the zero wind line (x-axis) at 1 hPa level (left panels: 15 June – 12 July; right panels: 29 June – 26 July) versus EP flux divergence (divEP, $ms^{-1}day^{-1}$, y-axis). a-b) Mean EP flux divergence at 50°S-40°S and between 1-10 hPa, times as given in the titles; c-f) Mean EP flux divergence at 60°S-40°S and between 50-70 hPa, times as given in the titles.

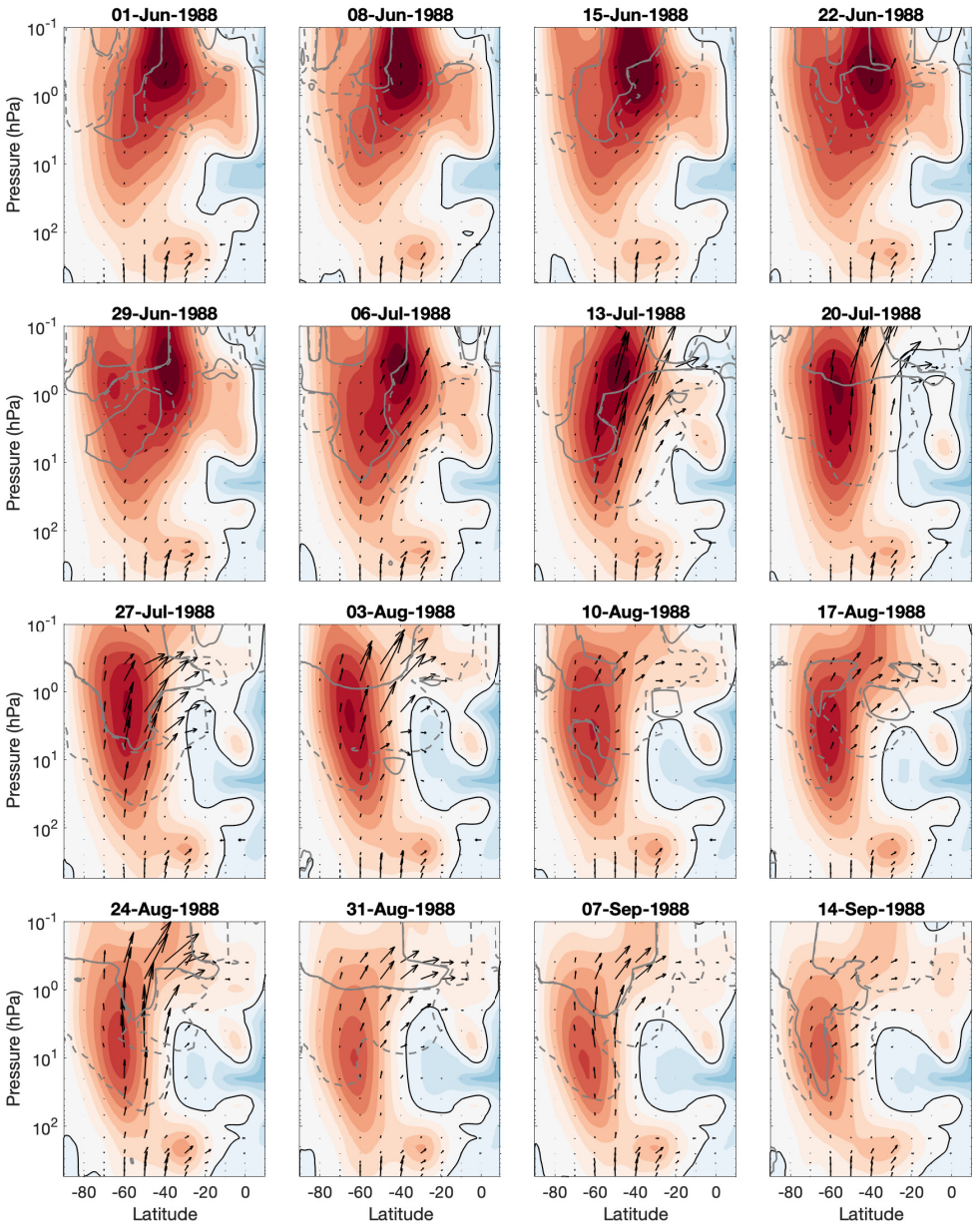

Figure 8. Supplement: As Figure 1 but for the year 1988.

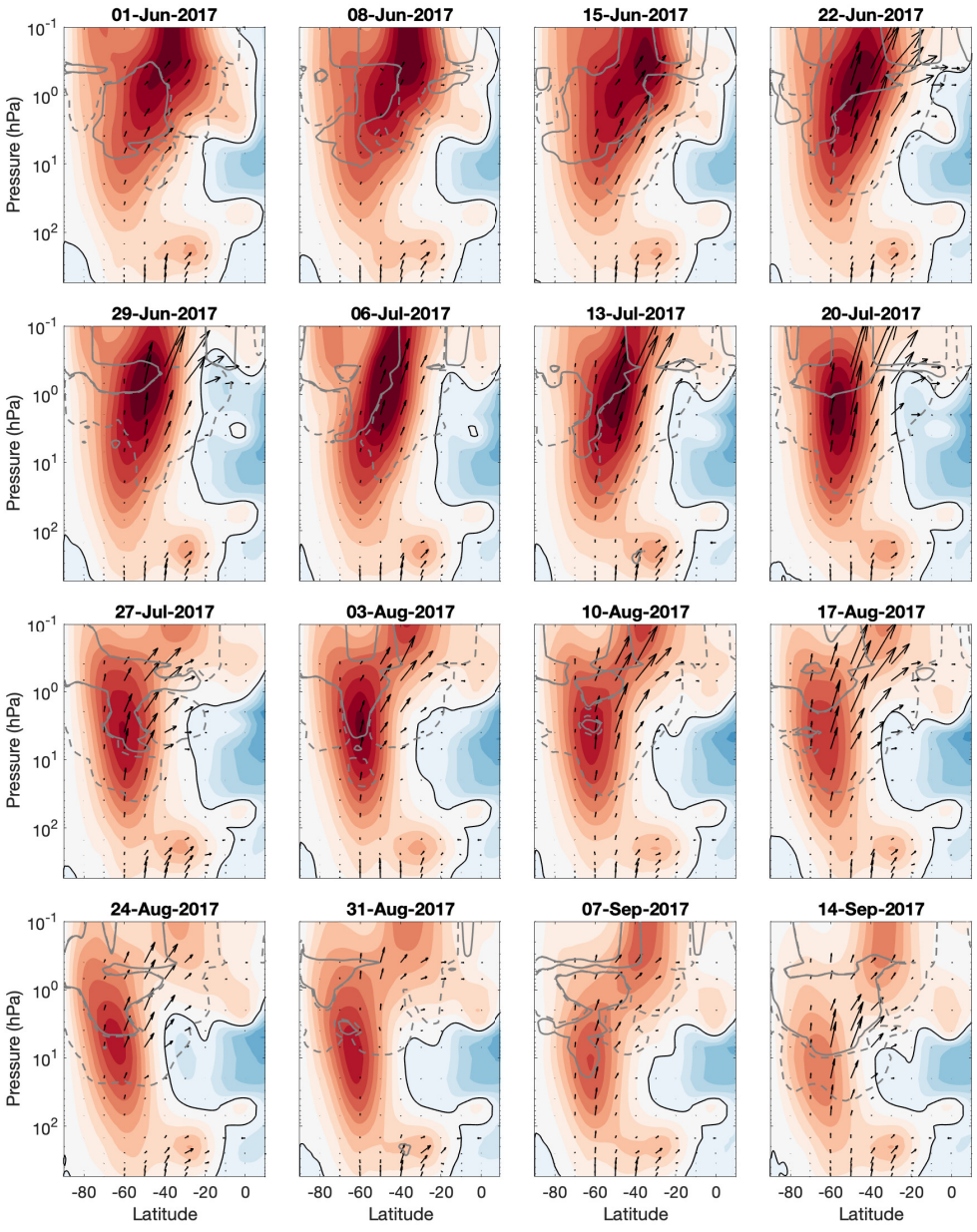

Figure 9. Supplement: As Figure 1 but for the year 2017.